Supporting Information

Schlichting and Preston 10.1073/pnas.1404396111

SI Methods and Results

Participants. Forty-eight right-handed volunteers (27 females; ages 20–33, mean ± SEM = 24.6 ± 0.5 y) participated in the experiment. Consent was obtained in accordance with an experimental protocol approved by the Institutional Review Board at the University of Texas at Austin. Participants received monetary compensation for their involvement in the study. Data from a total of 13 participants were excluded for the following reasons: hardware malfunction (n = 5), handedness concerns (n = 1), and low memory performance (n = 7). Low memory performance was defined as either (i) failure to subsequently recall more than 10% of new overlapping (BC) and nonoverlapping (XY) object–object associations studied in the scanner (n = 6) or (ii) failure to reach near-perfect performance on initial face–object (AB) associations (<80% cued recall accuracy; n = 1). Data from the remaining 35 participants were included in all analyses (21 females; ages 20–30, 24.1 ± 0.5 y).

Materials. Stimuli consisted of 60 grayscale images of famous faces (30 male and 30 female) and 240 grayscale images of common objects organized into 60 triads (denoted ABC) and 60 pairs (denoted XY) (Fig. 1*A*). All images were presented with verbal labels. ABC triads consisted of one face and two objects and were presented as overlapping AB and BC pairs, with the B item shared between pairs. That is, AB pairs always consisted of one famous face (A) paired with one object (B); the same object (B) was then paired with a different object (C) to form a BC pair. Nonoverlapping XY pairs consisted of two objects. All items were unique to their triad or pair, such that a single face or object image was a member of only one ABC triad or one XY pair. Four randomization groups were created to control for the organization of images into triads and pairs and viewing order. Objects were randomly assigned to item type (B, C, X, or Y), which determined both whether it belonged to a triad or pair and during which phase(s) it served as a recall cue (see below). An equal number of BC pairs associated with male and female faces (A) were presented within each of two BC encoding scans; no other constraints in item assignment or trial order were imposed. As described below, the order of BC encoding vs. XY encoding was counterbalanced across participants.

Memory Task. Participants completed a modified version of the associative inference task (Fig. 1*A*) (1–3). Before scanning, participants were trained to near-perfect performance on all 60 AB (face–object) pairs (Fig. 1*A*, blue). The goal of the pretraining phase was to create established memories for the AB pairs, such that overlapping BC information could then be encoded in relation to strong existing memories. The AB pretraining phase consisted of four study–test alternations. During the study phase, participants viewed each AB pair once [Fig. 1*A*, blue; 3.5-s stimulus, 0.5-s intertrial interval (ITI)]. "A" items (faces) were always shown on the right; "B" items (objects) were always on the left. Participants were encouraged to construct a visual or verbal story linking the items to aid memory but were not required to make any explicit response. Each study phase in the pretraining portion of the experiment lasted 4 min.

Following each study phase, participants completed a self-paced cued recall test (Fig. 1*A*, blue). The B item (object) was presented on the left side of the screen next to an empty box. Participants were asked to say aloud the name of the face that was paired with it. After either a verbal response had been produced or the trial was "passed," participants viewed a feedback display in which the correct image appeared in place of the empty box. Including the feedback displays, each pair was viewed a total of eight times during the pretraining phase.

After completing the initial AB pair pretraining, participants were transferred to the scanner after a delay (*SI Methods and Results*, *Delay and Encoding Order Analyses*). Importantly, at no time were participants made aware by the experimenter of the relationship between the pretraining phase and subsequent study and test tasks. That is, participants were not told that they would be learning overlapping associations in the scanner or that their memory for AB associations would later be probed via the inference (AC) test. Thus, whereas participants became aware of the overlap between the AB and BC pairs after the fact (all 35 reported awareness of this structure in a postexperiment questionnaire), there was no such expectation established before scanning. Once in the scanner, fMRI data were collected during 6 min of passive rest (Fig. 1*A*, yellow). During this time, a white fixation cross was displayed on a black screen. Participants were instructed to think about whatever they liked, while remaining awake and alert with their eyes open.

Following the initial post-AB rest scan, participants were scanned during encoding of overlapping BC (Fig. 1*A*, orange) and nonoverlapping XY pairs (Fig. 1*A*, green). Pairs were segregated by type into separate scans. There were a total of four slow event-related scans (two BC scans and two XY scans; 3.5 s stimulus, 8.5-s ITI). Participants were encouraged to construct a visual or verbal story while they encoded the new associations; no explicit responses were required. Each pair was presented just once, requiring rapid acquisition of associative information. C and Y objects were on the left; B and X objects were on the right. BC study scans always occurred in immediate succession, as did XY study scans. Encoding order of BC and XY scans was counterbalanced across participants. That is, for half of the participants, all BC pairs (scans 1 and 2) were learned before XY pairs (scans 3 and 4); for the other half, the order was reversed. Each study scan was 6 min long. Postencoding rest scans were acquired immediately following BC (e.g., after study scan 2) and XY (e.g., after study scan 4) learning (Fig. 1*A*, yellow). These scans were identical to the post-AB encoding rest scan described previously.

After the final rest scan, participants were taken out of the scanner to complete a cued recall test on BC and XY pairs (Fig. 1*A*, orange/green). C and Y items, presented on the left, served as probes. BC and XY test trials were randomly intermixed. Following completion of the BC/XY test, structure of the inferential (AC) associations was explained to participants. That is, participants were told that A and C items both paired with the same B item were indirectly related. Only two participants reported that they anticipated this inference test, even though all participants became aware of the overlap between the AB and BC associations during the BC study phase. They then completed a cued recall test on these surprise inference associations. The same items (C) served as probes, but this time participants were asked to name the indirectly related item (A, always a face). No feedback was provided during postscanning BC/XY or AC inference tests to prevent additional learning of the directly learned (BC/XY) associations.

Participants had the opportunity to practice the memory task before beginning the experiment. The practice included only nonoverlapping face–object associations using different stimuli from the main experiment.

Analysis of Behavioral Data. Cued recall responses were hand scored. Responses were scored as correct if the participant produced the correct label or, for famous faces, if they provided

a unique and accurate description of the person (e.g., by naming a film in which the actor was featured). We used this liberal criterion for recall because we found that participants would often recall a stimulus in great detail despite an inability to remember the specific verbal label. This type of recall performance was true for virtually only the A_{face} stimuli, and was particularly common early in the initial AB pair pretraining. For example, instead of recalling Daniel Radcliffe, the participant may state "the guy who plays Harry Potter." This criterion has been used in prior studies using a similar stimulus set and paradigm (4). A proportion correct was calculated for each participant, pair type (for AB, BC, XY, and AC), and repetition (for AB only).

The degree of facilitation versus interference exhibited was highly variable across participants (mean of XY − BC performance = 0.9%; SEM = 2.2%; range = −26.7–26.7%; Fig. S1*A*). Approximately half of the participants showed interference (n = 16 had numerically better XY than BC memory), whereas half showed facilitation (n = 15 had numerically better BC than XY memory). The remaining four participants had equal memory for BC and XY pairs.

Performance on BC pairs and AC inferences was highly correlated, both across participants (r_{33} = 0.98) and on a triad-by-triad basis within participant. Importantly, C items served as cues for both BC and AC test trials. Thus, using the example from Fig. 1*A*, the participant was first presented with CANDLE and asked to produce HARP as a test of BC memory. When the participant was again presented with CANDLE during the AC inference test, they should recall BRAD PITT. Because of this structure, AC inference can serve as an approximation of AB performance at the end of the memory task. We computed AC performance for only those triads for which the corresponding BC pair was recalled. Participants correctly recalled the vast majority of AC inferences when BC was correct (mean accuracy = 88.6%; median = 91.7%; SEM = 2.1%; range = 57.1–100%). This corresponded to on average just over two incorrect AC inferences when the overlapping BC was recalled (mean number of incorrect AC trials = 2.1; median = 2; SEM = 0.3; range = 0–8). These high levels of performance suggest that AB pairs were not forgotten over the course of the experiment.

To investigate the relationship between memory for the initial AB pairs and performance on overlapping BC pairs and AC inferences, we sorted triads according to when the AB pair was initially learned. We hypothesized that memory for those AB pairs learned early in the pretraining phase (e.g., that were correctly recalled on the first and all subsequent test blocks) may have stronger memory traces than for those learned late in pretraining (e.g., correctly recalled only on the final test block). An integrative encoding perspective predicts that stronger AB memories would support BC learning and AC inference. Thus, we would expect higher BC and AC performance when the corresponding AB pairs were learned early, relative to when they were learned late. Interestingly, interference theory might make the opposite prediction, with better BC and AC performance for later-learned AB pairs, as these weaker memories are less likely to interfere.

Accordingly, we sorted BC and AC test trials according to the AB test block on which the corresponding AB pair was correctly recalled for the first time. Due to the small number of participants (n = 16) who had any pairs that were first recalled on the fourth and final test block, we collapsed across pairs whose first recall occurred during blocks 3 and 4 for this analysis (referred to hereafter as block 1 AB pairs, block 2 AB pairs, and block 3/4 AB pairs). To be considered in this analysis, the AB pairs also had to be correctly recalled on all subsequent test blocks. That is, a block 1 AB pair was correctly recalled on blocks 1–4; a block 2 AB pair was correctly recalled on blocks 2–4; and a block 3/4 AB pair was either correctly recalled either on blocks 3 and 4 or only on block 4. We then assessed BC and AC performance as a function of AB acquisition time using a repeated measures ANOVA. All but three participants who had no block 3/4 AB pairs were included in this analysis (n = 32). We found a significant linear effect of AB memory strength on BC performance ($F_{1,31}$ = 5.19, P = 0.030; Fig. S1*B*, *Left* chart). This suggests that, consistent with an integrative encoding perspective, stronger initial memories are associated with superior encoding of overlapping content. Performing the same analysis for AC performance revealed a similar relationship ($F_{1,31}$ = 3.99, P = 0.055; Fig. S1*B*, *Right* chart), further suggesting that strong prior knowledge facilitates memory integration for subsequent flexible use.

Visual Localizer Task. After the memory task, participants completed a blocked design functional localizer during fMRI scanning to obtain neural patterns associated with viewing different types of visual stimuli. Participants viewed blocks of faces, objects, and scrambled objects while performing a one-back task. For each image, they pressed one of two buttons on a keypad to indicate whether the picture was new or a repeat of the immediately preceding picture. Responses were collected solely to ensure attention to the task and were not considered as part of the analysis. The images used in the localizer task were different from those used in the memory task. There were four blocks of each stimulus type per run, plus additional interleaved blocks of passive fixation. Blocks were 18 s long, yielding a total run length of 5 min. Three localizer scans were collected. Participants had the opportunity to practice the visual localizer task before beginning the experiment.

MR Data Acquisition. Imaging data were acquired on a 3.0T GE Signa MRI system (GE Medical Systems). All functional data were collected in 33, 3-mm thick oblique axial slices using an echo planar imaging (EPI) sequence [repetition time (TR) = 2,000 ms, echo time (TE) = 30.5 ms, flip angle = 73; 64 × 64 matrix, 3.75 × 3.75 mm in-plane resolution, bottom-up interleaved acquisition, 0.6 mm gap]. T2-weighted structural images were acquired in the same prescription as the functional images for the memory (TR = 3,200 ms, TE = 68 ms, 512 × 512 matrix, 0.46 × 0.46 mm in-plane resolution) and visual localizer (TR = 3,200 ms, TE = 68 ms, 256 × 256 matrix, 0.94 × 0.94 mm in-plane resolution) tasks. A T1-weighted 3D spoiled gradient recall (SPGR) structural volume (256 × 256 × 172 matrix, 1 × 1 × 1.3 mm voxels) was also collected to facilitate image coregistration and for automated parcellation using Freesurfer (http://surfer.nmr.mgh.harvard.edu/) (5).

fMRI Data Preprocessing. Functional data were preprocessed using FSL version 5.0.2 (FMRIB's Software Library, www.fmrib.ox.ac.uk/fsl). The first four volumes of all functional scans were discarded to allow for T1 stabilization. Motion correction was performed within each functional scan using MCFLIRT, by aligning all images in the run to the middle volume in the timeseries. Coregistration of functional data across runs was performed by calculating and applying the affine transformation from each run to a reference run using FLIRT, part of FSL. The 3D SPGR structural volume was registered to the functional reference run using the EPI registration utility (part of FLIRT) and then resampled to functional space. Brain extraction was performed on all structural and functional images using BET. With the exception of the group-level general linear models (GLMs), all analyses were done in the native functional space of each participant.

Regions of Interest. ***Anatomical region of interest definition.*** The hippocampal (HPC) and medial temporal lobe (MTL) cortices (entorhinal cortex, ERC; perirhinal cortex, PRC; and parahippocampal cortex, PHC) were delineated by hand on the 1-mm Montreal Neurological Institute (MNI) template brain and reverse normalized to each individual's functional space using Advanced Normalization Tools (ANTS) (6). Specifically, a nonlinear transformation was calculated from the MNI template brain to each participant's 3D SPGR volume. This warp was then

concatenated with the SPGR to functional space transformation calculated using FLIRT. After applying the transformation using ANTS, the anatomical MTL regions of interest (ROIs) were aligned to each participant's functional data.

Functional region of interest definition. Functional data from the localizer task were used to define face-sensitive voxels within the fusiform gyrus (i.e., fusiform face area, FFA). Analysis of fMRI data from the localizer task was carried out using FEAT (fMRI Expert Analysis Tool) version 6.00, part of FSL. The following prestatistics processing was applied: grand-mean intensity normalization of the entire 4D dataset by a single multiplicative factor; high-pass temporal filtering (Gaussian-weighted least-squares straight line fitting, with sigma = 64 s); and spatial smoothing [5 mm full width at half maximum (FWHM)]. FILM prewhitening was used. Stimulus presentation blocks were modeled as events of 18-s duration, with one regressor for each stimulus type (face, object, scrambled object, passive fixation). Stimulus regressors were convolved with the canonical (double-gamma) hemodynamic response function (HRF). Motion parameters calculated during the motion correction step and their temporal derivatives were added as additional confound regressors. Two measures of framewise data quality were also calculated to identify volumes that may be adversely impacted by motion artifacts: framewise displacement (FD) and the temporal derivative of the root-mean-square variance across voxels (DVARS) (7). FD measures the overall change in head position from one time point to the next and is calculated by summing the absolute values of the derivatives of the six motion parameters calculated during the realignment step. DVARS measures the overall change in image intensity from one time point to the next. This index is calculated as the root mean square of the derivatives of the timecourses across all voxels in the brain. Both FD and DVARS were added to the model as regressors of no interest (8). Additional regressors were created for each time point in which motion exceeded a threshold of both 0.5 mm for FD and 0.5% change in blood oxygen level-dependent (BOLD) signal for DVARS (plus one time point before and two time points after) (7). Temporal filtering was then applied to the model.

After modeling functional data within each run, the resulting statistical images were combined across localizer runs for each participant using fixed effects. As data were already coregistered across runs, no additional registration or spatial normalization was necessary. Face-selective regions were defined for each participant as those voxels responding more to faces than objects and scrambled objects. The procedure for FFA definition was as follows: we created 14-mm spheres centered at each participant's peak voxel (i.e., the maximum z statistic from the face > objects + scrambled objects contrast image) located within the posterior half of their Freesurfer-defined fusiform gyrus. This sphere was then masked with fusiform gyrus to restrict FFA to gray matter voxels. This method was used to ensure FFAs of approximately the same size across participants. This procedure was carried out separately for the left and right hemispheres; lateralized ROIs were then summed to create a bilateral FFA (ROI size range: 205–336 voxels, mean ± SEM = 288.7 ± 5.7 voxels). As ROI definition took place in the native functional space of each participant, no realignment or resampling was necessary.

Reactivation: Pattern Classification Analysis. Multivoxel pattern analysis (MVPA) was carried out using sparse multinomial logistic regression (SMLR) with a penalty term of 10 implemented in PyMVPA (9). The bilateral FFA mask described above was used for the main pattern classification analysis. In a follow-up analysis, we also interrogated reactivation within the posterior half of the fusiform gyrus defined on each participant (as above). By looking at this larger activation pattern, we were able to increase our statistical power. For each participant, a classifier was trained to differentiate patterns of activation associated with face, object, scrambled object, and passive fixation blocks using data from the visual localizer task. Following training, the classifier trained on localizer data from FFA was able to predict the visual content associated with new, unlabeled activation patterns from the same participant's brain with high accuracy (range: 70.4–96.1%, mean ± SEM: 84.4% ± 1.1% correct). Similar results were found for the posterior fusiform gyrus ROI (74.8–95.6%, 87.4 ± 0.7% correct).

The goal of the MVPA approach in the present study was to detect reactivation of previously encoded content (i.e., face information) during offline rest periods. To test the hypothesis that face information would be reactivated following the AB pair pretraining phase, we applied the trained classifier to each volume of the post-AB rest scan, acquired while the participant was viewing a fixation cross. The classifier estimates were extracted for each volume, yielding reactivation timecourses specific to each stimulus category for each participant.

A sliding window analysis was used to determine how the relationship between reactivation and BC memory performance changed across the duration of the post-AB rest scan. For each 60-TR window in the rest scan, a reactivation index was calculated for each participant as the average face evidence across the window. Whereas we focus primarily on face evidence in the main text (Fig. S2, *Upper Left*), this measure was also calculated for the remaining stimulus categories, for which we did not see any relationship to behavior (Fig. S2, *Upper Right*). This index was then related to BC performance across participants using partial correlation (controlling for XY performance). This resulted in a partial correlation value (r) that was Fisher transformed (z) and assigned to the middle TR of the window. We defined 95% confidence intervals on the partial correlation statistic for each window using a bootstrapping procedure as follows: for each of 1,000 iterations, a group of 35 participants was drawn randomly with replacement from our sample. We then repeated the pattern classification analysis with this simulated group of participants, yielding a partial correlation statistic (Fisher's z) for each analysis. After repeating this procedure 1,000 times, partial correlation statistics were sorted and confidence intervals were drawn at the 25th (the upper 2.5%) and 975th (lower 97.5%) z values. The window was then shifted by one TR and the entire procedure was repeated. This analysis was also performed separately for individual relationships with BC and XY performance using Pearson's correlation (Fig. S2, *Lower* row). As the relationship between reactivation and performance was unique to the beginning of the scan, the results reported in the main text (*Results*, *Face Reactivation During Rest*) and below focus on how reactivation relates to behavior during the first 60-TR window (Fig. 2, *Lower*).

Individual relationships with BC, AC, and XY performance were assessed in the first 60-TR window using Pearson's correlation. We also compared the separate relationships of reactivation with BC and AC with that of XY using the Hotelling–Williams procedure (10, 11), a statistical test that accounts for shared variance among related measures. The partial correlation between reactivation and memory facilitation during the post-AB rest was driven by a numerically positive relationship between reactivation and BC performance ($r_{33} = 0.20$, $P = 0.239$); and a numerically negative relationship between reactivation and XY performance ($r_{33} = -0.07$, $P = 0.681$; Figs. S2, *Lower* row and S3*A*). Whereas neither relationship was statistically significant on its own, they were significantly different from one another (Hotelling–Williams test; $t_{32} = 2.74$, $P = 0.010$). Tracking BC performance, the relationship between reactivation and AC performance was also positive, although it too did not reach statistical significance ($r_{33} = 0.18$, $P = 0.310$; Fig. S3*A*). The relationship between reactivation and AC performance also differed significantly from XY (Hotelling–Williams test; $t_{32} = 2.50$, $P = 0.018$). Importantly, we present these data with the caveat that the individual relationships are

difficult to interpret, as they include effects attributable to general associative memory ability.

Using the entire posterior fusiform gyrus ROI, the partial correlations between reactivation and BC performance (r_{32} = 0.38, P = 0.028) and reactivation and AC performance (r_{32} = 0.37, P = 0.032) remained statistically significant. Moreover, the individual relationships (Fig. S3*B*) between reactivation and BC performance (r_{33} = 0.37, P = 0.028) and reactivation and AC performance (r_{33} = 0.36, P = 0.032) were significant in this larger ROI, whereas the relationship with XY performance remained nonsignificant (r_{33} = 0.19, P = 0.282). The difference in the reactivation–performance relationships for both BC and XY (Hotelling–Williams test; t_{32} = 1.81, P = 0.079) and AC and XY (Hotelling–Williams test; t_{32} = 1.78, P = 0.085) trended toward significance in this expanded region.

We also performed several control analyses that leveraged the post-XY encoding rest period to investigate the specificity of this reactivation–performance relationship to the post-AB rest. These analyses were performed to assess the hypothesis that the observed measures relate specifically to memory integration and are modulated by experience (i.e., they are not stable within an individual over time). For these analyses, we treated the post-XY rest as a baseline period. We believe this serves as an appropriate control in the present study for two reasons. First, of the three rest scans acquired in the present study (post-AB, post-BC, and post-XY encoding), the post-XY encoding rest is the most removed from the demands of overlapping encoding (e.g., memory integration or interference resolution). For this reason, it is likely that this period would reflect the most recent experience: encoding of object–object (XY) associations that did not overlap with the critical A_{face} information. Second, whereas post-XY encoding rest may not reflect "true" baseline activity in the traditional sense, it is a stringent and appropriate control for studying the phenomenon of interest. That is, as we expect post-XY encoding rest to reflect persistence of signatures associated with simple associative encoding, any additional effects observed during post-AB encoding rest are all of the more likely to relate specifically to overlapping encoding. Importantly, as our neural measures are defined specifically to index processing of face-related memories, we would not expect the degree of FFA reactivation during the post-XY period to relate to XY performance.

Accordingly, we interrogated the relationship between FFA reactivation during post-XY encoding rest and memory performance. One alternative account of our findings is that the observed neural measures simply reflect general associative memory ability and are unrelated to memory integration in particular. To assess this possibility, we related FFA reactivation during the post-XY period to general associative memory performance (XY) across participants. We found that face reactivation in FFA following XY encoding was not related to general associative memory (XY) performance (r_{33} = 0.11, P = 0.52), rendering an account based purely on general associative memory signatures improbable. A second alternative account is that stable individual differences in reactivation are associated with superior memory integration. If this were indeed the case, one would expect that reactivation measures from an unrelated rest period (e.g., post-XY encoding rest) should predict BC performance after controlling for XY. This was not the case in our data; we observed no relationship between post-XY reactivation and BC (r_{32} = −0.06, P = 0.747) or AC (r_{32} = −0.09, P = 0.587) performance after controlling for XY performance using partial correlation. Thus, these control analyses are consistent with the notion that enhanced reactivation during rest confer a specific behavioral advantage on subsequent learning of related content.

Post-XY reactivation was also subtracted from post-AB reactivation for each participant (12); these difference scores were then related to performance as described previously. The goal of this approach was to account for differences in baseline connectivity across participants. This analysis replicated our prior findings for both FFA and anatomically defined posterior fusiform gyrus ROIs. Specifically, reactivation in FFA was related to BC memory (r_{32} = 0.33, P = 0.054) and inference (r_{32} = 0.34, P = 0.050) after controlling for general associative memory performance. Moreover, the correlations between reactivation and BC (Hotelling–Williams test; t_{32} = 2.14, P = 0.040) and AC (Hotelling–Williams test; t_{32} = 2.18, P = 0.037) performance each differed significantly from the relationship between reactivation and XY performance. In posterior fusiform gyrus, reactivation also maintained its significant relationships with BC memory (r_{32} = 0.39, P = 0.023) and inference (r_{32} = 0.42, P = 0.013) after controlling for XY performance. In addition, the individual relationships between reactivation and BC performance (r_{33} = 0.39, P = 0.022) and AC inference (r_{33} = 0.40, P = 0.017)—but not XY performance (r_{33} = 0.20, P = 0.259)—were significant. The difference between BC and XY correlations with reactivation approached significance (Hotelling–Williams test; t_{32} = 1.87, P = 0.071); its relationship with AC was significantly different from XY (Hotelling–Williams test; t_{32} = 2.13, P = 0.041).

Functional Connectivity. Functional connectivity was examined using two approaches: first, a timeseries correlation within anatomically and functionally defined ROIs and second, a voxelwise regression approach using FFA as a seed region.

Timeseries correlation analysis. For each participant, functional data from the post-AB rest scan were high-pass filtered with a cutoff of 0.009 Hz, which has been used in previous studies examining rest-phase connectivity (12, 13). For each FFA and MTL ROI, the first eigenvariate of the signal across all voxels in the mask was extracted across the full 6 min (180 TRs) of the post-AB rest period. For each participant, the FFA timeseries was then correlated with the timeseries from each MTL ROI. This procedure resulted in four correlation values (r) per participant (FFA–HPC, FFA–ERC, FFA–PRC, and FFA–PHC), representing the degree of functional connectivity between FFA and each of the MTL ROIs during the post-AB rest period. For each pair of ROIs, connectivity was related to BC and AC performance across participants using partial correlation (controlling for XY performance). Individual relationships with BC, AC, and XY performance were also assessed using Pearson's correlation. Relationships to BC and XY, and AC and XY, were compared using the Hotelling–Williams test (10, 11). The individual relationships between FFA–HPC connectivity and BC (r_{33} = 0.12, P = 0.500), AC (r = 0.09, P = 0.59), and XY (r_{33} = −0.13, P = 0.467) performance did not reach statistical significance. However, the connectivity–performance relationships for BC and XY performance were significantly different from one another (Hotelling–Williams test; t_{32} = 2.36, P = 0.024), as was the difference between relationships with AC and XY performance (Hotelling–Williams test; t_{32} = 2.18, P = 0.037).

We also repeated this analysis after regressing out potential sources of noise from the resting state data. Specifically, we extracted the first eigenvariate of the signal across the duration of the rest scan in anatomically defined white matter and lateral ventricle ROIs. The signal from these two ROIs and their temporal derivatives were used to construct a GLM along with motion parameters, FD, DVARS, and their temporal derivatives, and timepoints with excessive motion (as described above in *SI Methods and Results*, *Functional region of interest definition*). The high-pass filtered data from the previously described step were then regressed on these noise sources, and the first eigenvariate was extracted from the resulting data (i.e., the residual timeseries). As in the above-described analysis, each participant's FFA timeseries was then correlated with their MTL timeseries, resulting in four indices representing functional connectivity between FFA and the four MTL regions. These

measures were then related to performance using partial correlation and Pearson's correlation. The relationship between FFA–HPC connectivity and BC learning ($r_{32} = 0.30$, $P = 0.088$) and connectivity and AC inference ($r_{32} = 0.30$, $P = 0.089$) after controlling for XY memory approached significance.

We also calculated connectivity measures for the post-XY encoding rest period for the purposes of the control analyses. Connectivity was related to XY performance using Pearson's correlation and to BC and AC performance controlling for XY using partial correlation. We found no relationship between FFA–HPC connectivity following XY encoding and XY memory performance ($r_{33} = -0.22$, $P = 0.20$), suggesting that this signature does not simply reflect general associative memory ability. There was also no relationship between connectivity and BC ($r_{32} = -0.11$, $P = 0.538$) or AC ($r_{32} = -0.11$, $P = 0.534$) performance after controlling for XY.

To control for possible individual differences in baseline FFA–HPC connectivity, post-XY connectivity was also subtracted from post-AB connectivity for each participant (12). The resulting difference scores were then related to performance as above. The difference scores showed a significant relationship with BC ($r_{32} = 0.40$, $P = 0.018$) and AC ($r_{32} = 0.38$, $P = 0.025$) performance after controlling for general associative memory, as well as significant individual relationships with BC ($r_{33} = 0.35$, $P = 0.040$) and AC ($r_{33} = 0.33$, $P = 0.052$) performance. There was no association between FFA–HPC connectivity and XY performance ($r_{33} = 0.13$, $P = 0.444$). BC and XY (Hotelling–Williams test; $t_{32} = 2.10$, $P = 0.043$); and AC and XY (Hotelling–Williams test; $t_{32} = 1.98$, $P = 0.056$) relationships with FFA–HPC connectivity also differed from one another.

Seed-based analysis. This analysis interrogated activation within MTL (inclusive of HPC, ERC, PRC, and PHC) for voxels that showed rest-phase connectivity with FFA that related to subsequent performance. We performed this analysis to account for the potential heterogeneity in response profiles within the MTL, thereby complementing above ROI approach above. Each participant's high-pass filtered functional data were spatially smoothed (5-mm FWHM). The FFA timeseries and its first temporal derivative were entered into a GLM, along with motion-related confound regressors (motion parameters, FD, DVARS, and their temporal derivatives and timepoints with excessive motion). The resulting parameter estimate image for each participant reflected the degree to which activation in each MTL voxel tracked with FFA activation across the post-AB rest scan. We then warped these images to the 1-mm MNI template using ANTS (6) and combined them across participants using a group-level GLM as follows: We constructed the group-level model with both BC and XY performance as covariates. We were specifically interested in those MTL voxels whose connectivity with FFA was modulated by individual differences in BC performance (after covarying out XY performance), as well as those voxels that tracked more with BC than XY performance (BC > XY contrast). Voxelwise statistics were calculated within MTL using permutation tests implemented in FSL. We first applied an uncorrected voxelwise threshold of $P < 0.025$ to the group statistics images. We then corrected for multiple comparisons within the MTL using a small volume correction procedure to determine the cluster size corresponding to a cluster-corrected threshold of $P < 0.05$. This calculation was carried out using 3dClustSim, part of AFNI (14). The 3dClustSim performs Monte Carlo simulations that take into account the size and shape of the ROI as well as the smoothness of the data in determining a critical cluster size. Cluster sizes that occurred with a probability of <0.05 across 2,000 simulations were considered statistically significant. This procedure yielded a critical cluster size of 326 (1 mm^3) voxels for the MTL ROI (Fig. 3*B* and Fig. S5). We also repeated the seed-based analysis on the residuals from the nuisance regressed analysis described above. As motion-related nuisance signals had already been removed, each model included only the FFA timeseries and its temporal derivative. All other steps were identical to those carried out on the high-pass filtered data (Fig. S4).

Multiple Regression Analysis. Multiple linear regression analyses were performed to further assess the degree to which reactivation and connectivity indices were independently related to performance. Two regression models were run: one with BC performance as the dependent variable and one with AC performance as the dependent variable. Reactivation, connectivity, and XY performance measures for each participant were entered into the regression as predictors. Participants were treated as a random effect. These findings are presented in *Results*, *Multiple Regression*.

Univariate Analysis. Analysis of fMRI data from the memory task was carried out using FEAT (fMRI Expert Analysis Tool) version 6.00, part of FSL. As with the localizer data, the following prestatistics processing was applied: grand-mean intensity normalization of the entire 4D dataset by a single multiplicative factor; high-pass temporal filtering (Gaussian-weighted least-squares straight line fitting, with sigma = 64 s); and spatial smoothing (5-mm FWHM). FILM prewhitening was used. Encoding trials were sorted based on subsequent memory in the cued recall test to create four conditions: BC encoding trials that were later correct, BC encoding trials that were later incorrect, XY encoding trials that were later correct, and XY encoding trials that were later incorrect. Stimulus presentations were modeled as events with 3.5-s durations, with one regressor for each of the four conditions. The model was convolved with the canonical (double gamma) HRF. Motion parameters calculated during the motion correction step and their temporal derivatives were added as additional regressors of no interest. As described above, FD, DVARS, and individual regressors for time points exceeding FD and DVARS thresholds were added to the model to additionally account for motion effects (7, 8). Temporal filtering was applied to the model.

After modeling functional data within each run, the resulting statistics images were warped to the 1-mm MNI template brain using ANTS (6). The warped images were combined across encoding runs for each participant using fixed effects and then across the group using mixed effects. Correction for multiple comparisons was carried out on group-level voxelwise statistical images according to cluster-based Gaussian random field theory (15), with a cluster-forming threshold of $z > 2.3$ and a whole-brain corrected cluster significance level of $P < 0.05$.

In addition to a group mean model, two models with covariates were created to investigate how individual differences in rest-phase reactivation and functional connectivity relate to subsequent neural activation during learning of BC and XY pairs. For each of these two models, a second regressor was created containing FFA reactivation and FFA–HPC connectivity indices, respectively, for every participant. We then examined regions whose activation was modulated by these covariates. Correction for multiple comparisons was performed as described above.

Delay and Encoding Order Analyses. Participants experienced a variable delay between AB pretraining and the post-AB encoding rest scan (median delay length = 22 min, SEM = 1.76, range = 15–58). Moreover, as encoding order was counterbalanced across participants, there was also a difference in time between the initial learning of the AB pairs and subsequent encoding over the overlapping BC pairs. To rule out these potential confounds, we performed two analyses. First, we assessed the continuous relationship between delay duration and FFA reactivation and delay duration and FFA–HPC connectivity measures using Pearson's correlation. There was no relationship

across the group between duration of the delay and the post-AB neural measures of interest (FFA reactivation: $r_{33} = 0.10$, $P = 0.58$; FFA–HPC connectivity: $r_{33} = 0.19$, $P = 0.27$), suggesting that the length of the delay did not significantly influence the degree to which these processes were engaged.

We also performed one-way analyses of covariance (ANCOVA) to interrogate whether the observed relationships between neural measures and performance differed significantly as a function of encoding order. The neural measure (FFA reactivation or FFA–HPC connectivity) served as the predictor variable; the behavioral measure served as the response. Encoding order was the grouping variable. Encoding order did not significantly impact the relationships between connectivity (main effects and interactions; all $F_{1,31} < 1.02$, all $P > 0.32$) or reactivation (main effects and interactions; all $F_{1,31} < 0.32$, all $P > 0.57$) and BC or AC performance controlling for XY performance. Individual relationships between reactivation and performance (BC: both $F_{1,31} < 0.49$, $P > 0.49$; AC: both $F_{1,31} < 0.64$, $P > 0.43$; XY: both $F_{1,31} < 1.40$, $P > 0.24$) and FFA–HPC connectivity and performance (BC: both $F_{1,31} < 0.58$, $P > 0.45$; AC: both $F_{1,31} < 0.32$, $P > 0.58$; XY: both $F_{1,31} < 0.14$, $P > 0.72$) were also not modulated by encoding order.

1. Preston AR, Shrager Y, Dudukovic NM, Gabrieli JDE (2004) Hippocampal contribution to the novel use of relational information in declarative memory. *Hippocampus* 14(2):148–152.
2. Zeithamova D, Preston AR (2010) Flexible memories: Differential roles for medial temporal lobe and prefrontal cortex in cross-episode binding. *J Neurosci* 30(44): 14676–14684.
3. Zeithamova D, Dominick AL, Preston AR (2012) Hippocampal and ventral medial prefrontal activation during retrieval-mediated learning supports novel inference. *Neuron* 75(1):168–179.
4. Kuhl BA, Rissman J, Chun MM, Wagner AD (2011) Fidelity of neural reactivation reveals competition between memories. *Proc Natl Acad Sci USA* 108(14):5903–5908.
5. Desikan RS, et al. (2006) An automated labeling system for subdividing the human cerebral cortex on MRI scans into gyral based regions of interest. *Neuroimage* 31(3): 968–980.
6. Avants BB, et al. (2011) A reproducible evaluation of ANTs similarity metric performance in brain image registration. *Neuroimage* 54(3):2033–2044.
7. Power JD, Barnes KA, Snyder AZ, Schlaggar BL, Petersen SE (2012) Spurious but systematic correlations in functional connectivity MRI networks arise from subject motion. *Neuroimage* 59(3):2142–2154.
8. Schonberg T, et al. (2014) Changing value through cued approach: An automatic mechanism of behavior change. *Nat Neurosci* 17(4):625–630.
9. Hanke M, et al. (2009) PyMVPA: A python toolbox for multivariate pattern analysis of fMRI data. *Neuroinformatics* 7(1):37–53.
10. Hotelling H (1940) The selection of variates for use in prediction with some comments on the general problem of nuisance parameters. *Ann Math Stat* 11:271–283.
11. Williams EJ (1959) The comparison of regression variables. *J R Stat Soc, B* 21:396–399.
12. Tambini A, Ketz N, Davachi L (2010) Enhanced brain correlations during rest are related to memory for recent experiences. *Neuron* 65(2):280–290.
13. Fox MD, et al. (2005) The human brain is intrinsically organized into dynamic, anticorrelated functional networks. *Proc Natl Acad Sci USA* 102(27):9673–9678.
14. Cox RW (1996) AFNI: Software for analysis and visualization of functional magnetic resonance neuroimages. *Comput Biomed Res* 29(3):162–173.
15. Worsley KJ, et al. (2002) A general statistical analysis for fMRI data. *Neuroimage* 15(1):1–15.

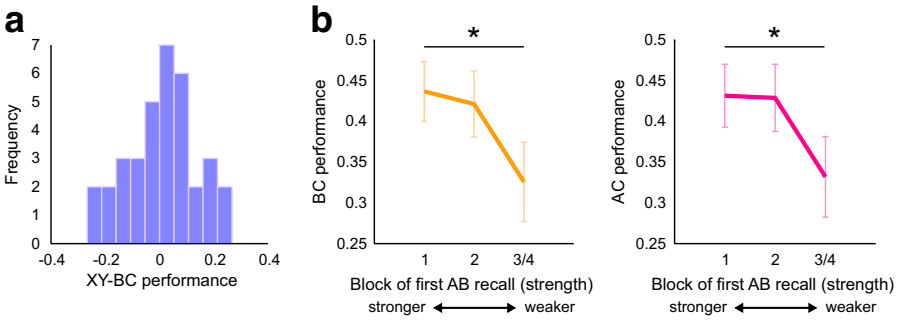

Fig. S1. Behavioral performance. (*A*) Histogram depicting distribution of behavioral interference in our sample (displayed as the difference between XY and BC performance). Positive values indicate better XY than BC performance, evidencing interference of prior AB knowledge on new encoding; negative values indicate better BC than XY performance, indicating AB knowledge-related facilitation. (*B*) BC performance (orange; *Left*) and AC performance (pink; *Right*) as a function of AB memory strength. AB pairs were sorted according to whether they were correctly recalled initially on the first, second, or third/fourth pretraining test block (*x* axis). BC and AC performance was then computed separately for these groups of triads (*y* axis). There was a significant linear effect of block of first AB recall on both BC and AC performance; participants demonstrated better memory for those AB pairs learned earlier in the pretraining phase, suggesting that strong AB memories facilitate new learning. Significant linear effects denoted by asterisks.

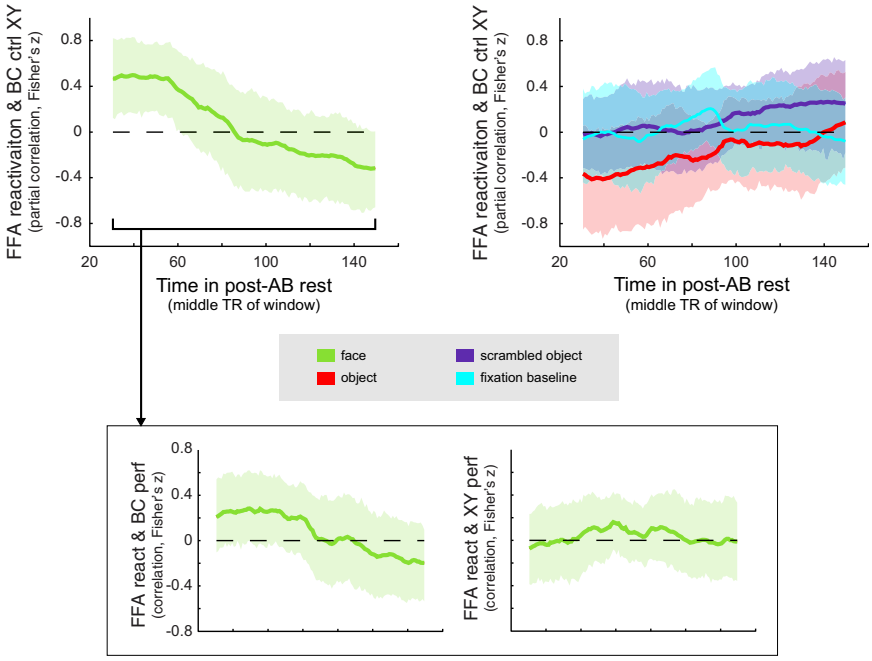

Fig. S2. Relationship between FFA reactivation and memory over time. (*Upper* row) Relationship between FFA reactivation and BC performance controlling for XY performance over time. For each 60-TR window, we calculated the partial correlation between mean classifier evidence for all four stimulus categories (face, *Left*; object, scrambled object, and fixation baseline, *Right*) in FFA and BC performance, controlling for XY performance. Partial correlation values (*r*) were Fisher transformed (*z*) and assigned to the middle TR of the window. Data are plotted as partial correlation values (*y* axis) over time (middle TR; *x* axis). Face evidence (*Left*; green) was significantly related to BC performance (controlling for XY performance) at the beginning of the rest scan; this relationship decreased over time. (*Right*) Relationship between classifier evidence for remaining stimulus categories (*Right*; object, red; scrambled object, purple; fixation baseline, cyan) and performance. There was no significant relationship between evidence for any of these stimulus types and BC performance controlling for XY across the duration of the rest scan. (*Lower* row) Individual relationships between FFA reactivation and BC and XY performance over time. We calculated separate Pearson's correlations between mean classifier evidence for faces in FFA and BC performance (*Left*) and XY performance (*Right*) for each window. As above, correlation values (*r*) were Fisher transformed and assigned to the middle TR. Data are plotted as correlation values (*y* axis) over time (middle TR; *x* axis). The significant partial correlation (*Upper Left*, early in scan) was driven by a positive relationship with BC performance early in the scan and no relationship to XY performance. For all plots, shaded region represents 95% bootstrapped confidence intervals.

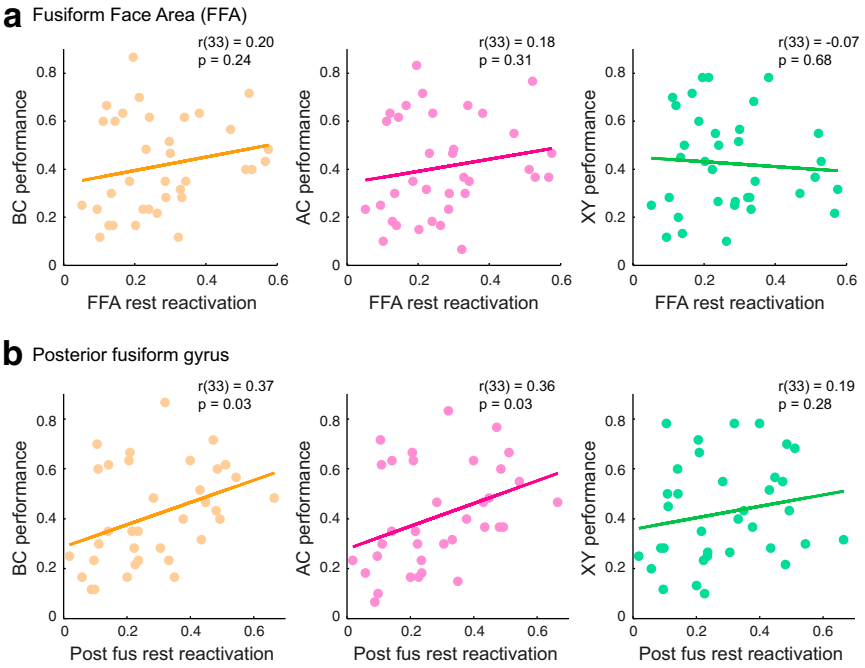

Fig. S3. Individual relationships between reactivation and performance for FFA (*A*) and posterior fusiform gyrus (*B*) ROIs. (*A*) Relationships between FFA reactivation (*x* axes) and BC (*Left*; orange), AC (*Center*; pink), and XY (*Right*; green) performance (*y* axes). BC and AC performance were positively (although nonsignificantly) associated with reactivation; XY was negatively (although nonsignificantly) associated with reactivation. (*B*) Relationships between posterior fusiform reactivation and performance. Data are displayed as in *A*. Both BC and AC performance showed significantly positive relationships with reactivation, such that greater reactivation was associated with superior performance. There was also a numerically positive but nonsignificant relationship with XY. For both *A* and *B*, results were similar after subtracting baseline reactivation levels derived from the post-XY encoding rest period (not depicted) (see *SI Methods and Results, Reactivation: Pattern Classification Analysis*). All statistics reflect Pearson's correlations.

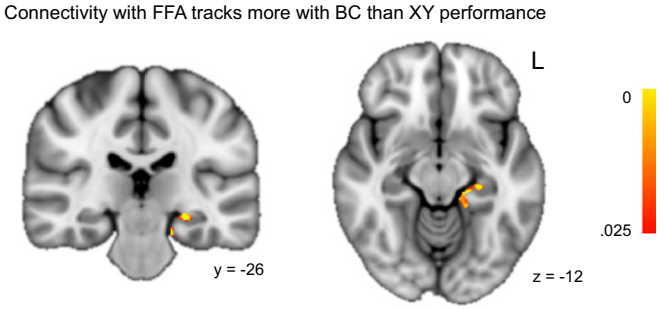

Fig. S4. MTL regions for which connectivity with FFA during rest is significantly more predictive of BC than XY performance. These results depict analysis performed on rest data following nuisance regression. This contrast revealed a cluster in left hippocampus (−17, −30, −20) that overlapped with the results from the high-pass filtered rest data (Fig. 3*B*). Cluster is significant after correction for multiple comparisons within the MTL. Color bar indicates uncorrected voxelwise *P* value. Coordinates are in millimeters.

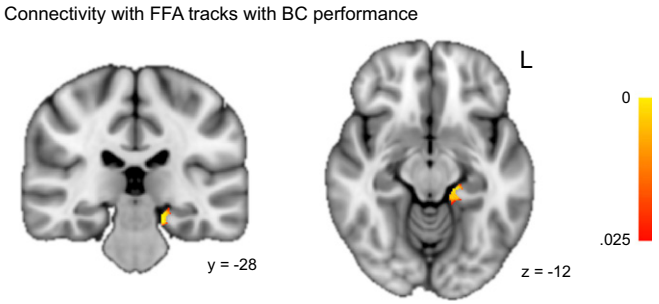

Fig. S5. MTL regions for which connectivity with FFA during rest significantly predicts BC performance. Left hippocampus (−18, −29, −13) was the only region for which greater post-AB rest-phase connectivity with FFA was associated with superior BC performance. Cluster is significant after correction for multiple comparisons within the MTL. No regions showed a positive relationship with XY performance. Color bar indicates uncorrected voxelwise *P* value. Coordinates are in millimeters.

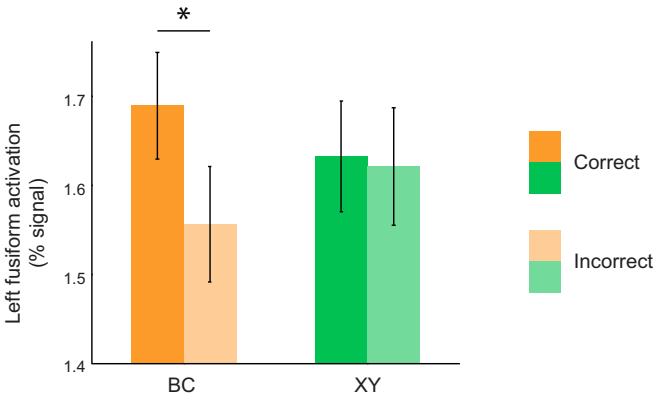

Fig. S6. Encoding activation in left fusiform gyrus relates to memory for overlapping BC but not XY pairs. Parameter estimates were extracted from regions of left fusiform gyrus identified as showing a significant subsequent recall by condition interaction (correct > incorrect × BC > XY) displayed in Fig. 4*A*. Estimates were converted to percent signal and are shown separately for BC pairs subsequently remembered (dark orange); BC pairs subsequently forgotten (light orange); XY pairs subsequently remembered (dark green); and XY pairs subsequently forgotten (light green). The significant interaction in this region was driven by a strong subsequent memory effect for BC pairs (paired *t* test; $t_{34} = 6.23$, $P = 4.4 \times 10^{-7}$; dark vs. light orange bars) but not XY pairs ($t_{34} = 0.49$, $P = 0.625$; dark vs. light green bars). Asterisk indicates significant difference at $P < 0.05$.